Clathrin-mediated endocytosis is essential in *Trypanosoma brucei*

Clare L.Allen, David Goulding and Mark C.Field[1]

Wellcome Trust Laboratories for Molecular Parasitology, Department of Biological Sciences, Imperial College, Exhibition Road, London SW7 2AY, UK

[1]Corresponding author
e-mail: mfield@imperial.ac.uk

In *Trypanosoma brucei*, the plasma membrane is dominated by glycosylphosphatidylinositol (GPI)-anchored proteins. Endocytic activity correlates with expression levels of the clathrin heavy chain TbCLH, and additional evidence suggests that rapid endocytosis may play a role in evasion of the immune response. TbCLH is present on both endocytic vesicles and post-Golgi elements, suggesting a similar range of functions in trypanosomes to higher eukaryotes. We have assessed the role of TbCLH using RNA interference (RNAi). Suppression of TbCLH expression results in rapid lethality in the bloodstream stage, the form most active for endocytosis. The flagellar pocket, the site of both endocytosis and exocytosis, becomes massively enlarged, suggesting that membrane delivery is unaffected but removal is blocked. Endocytosis in TbCLHRNAi cells is essentially undetectable, suggesting that clathrin-mediated mechanisms are the major route for endocytosis in *T.brucei* and hence that GPI-anchored proteins are endocytosed by clathrin-dependent pathways in trypanosomes. In contrast, a massive internal accumulation of vesicles and significant alterations to trafficking of a lysosomal protein were observed in the procyclic stage, indicating developmental variation in clathrin function in trypanosomes.

Keywords: clathrin/endocytosis/post-Golgi transport/protein sorting/vesicle trafficking

Introduction

In higher eukaryotic systems, endocytosis of cell surface components is achieved by at least two mechanisms, principally defined by requirement for, or independence from, the membrane coat protein clathrin (Nichols and Lippincott-Schwartz, 2001). The clathrin-dependent pathway is well characterized in metazoans, yeasts and plants and involves a large number of protein factors, together with membrane lipids (Takei and Haucke, 2001). In yeast, the pathway is non-essential in culture when cells are allowed to adapt to clathrin absence (Seeger and Payne, 1992). In vertebrate cells, clathrin deficiency invokes an apoptotic pathway (Wettey *et al.*, 2002), suggesting an anti-apoptotic role. Most interestingly, in chick DKO-R cells lacking the apoptotic pathway, clathrin knockouts are

viable, suggesting that clathrin-mediated endocytosis is non-essential in metazoans (Wettey *et al.*, 2002). In both yeast and vertebrates, comparatively minor alterations in transport are observed in cells lacking functional clathrin (Yeung *et al.*, 1999; Wettey *et al.*, 2002), which is perhaps counter-intuitive, given the number of pathways in which clathrin has been implicated and the extensive protein–protein interaction networks that centre on clathrin (e.g. Costaguta *et al.*, 2001; Takei and Haucke, 2001).

Besides clathrin, the most important components of clathrin-mediated endocytosis include dynamin (Merrifield *et al.*, 2002), epsin (Ford *et al.*, 2002) and a heterotetrameric adaptor complex, AP-2, which binds both clathrin and cytoplasmic tyrosine-based signals on transmembrane proteins (Boehm and Bonifacino, 2002). Other factors are also important (Takei and Haucke, 2001). Clathrin also participates in *trans*-Golgi-derived transport and endosomal sorting; here, clathrin operates in the context of a distinct set of proteins, including adaptor complexes 1, 3 and, possibly, 4 (Boehm and Bonifacino, 2002).

Clathrin-independent mechanisms are less well characterized; the best-understood system involves caveolin. The caveolin-mediated mechanism also appears to require dynamin (Le *et al.*, 2002; Magalhaes *et al.*, 2002), but other clathrin pathway factors are most likely not involved. Most importantly, for the majority of cell types and proteins studied, the clathrin-independent pathway is responsible for endocytosis of glycosylphosphatidylinositol (GPI)-anchored proteins (Benting *et al.*, 1999; Wang *et al.*, 2002). As these molecules lack cytoplasmic protein domains, association of this class of protein with lipid rafts provides an explainable mechanism for GPI-anchored protein endocytosis. All pathways appear to converge within the endocytic system (Magalhaes *et al.*, 2002; Sabharanjak *et al.*, 2002).

Trypanosoma brucei provides a unique opportunity for insight into endocytic systems, as the plasma membrane is dominated by GPI-anchored proteins, endocytosis is developmentally regulated and membrane trafficking is highly polarized, with all endocytosis taking place from the flagellar pocket (Morgan *et al.*, 2002a,b). Expression of the trypanosome clathrin heavy chain, TbCLH, correlates with endocytic activity (Morgan *et al.*, 2001), but extensive searches of the *T.brucei* genome database have failed to detect trypanosome AP-2 complex subunits (Ilgoutz and McConville, 2001; Morgan *et al.*, 2002b). Despite this, ultrastructural evidence indicates that GPI-anchored proteins are endocytosed by clathrin-coated vesicles (Grunfelder *et al.*, 2003). There is no direct evidence for clathrin-independent mechanisms; despite observations of detergent-resistant membrane-like structures in trypanosomatids, including *T.brucei* (Denny *et al.*,
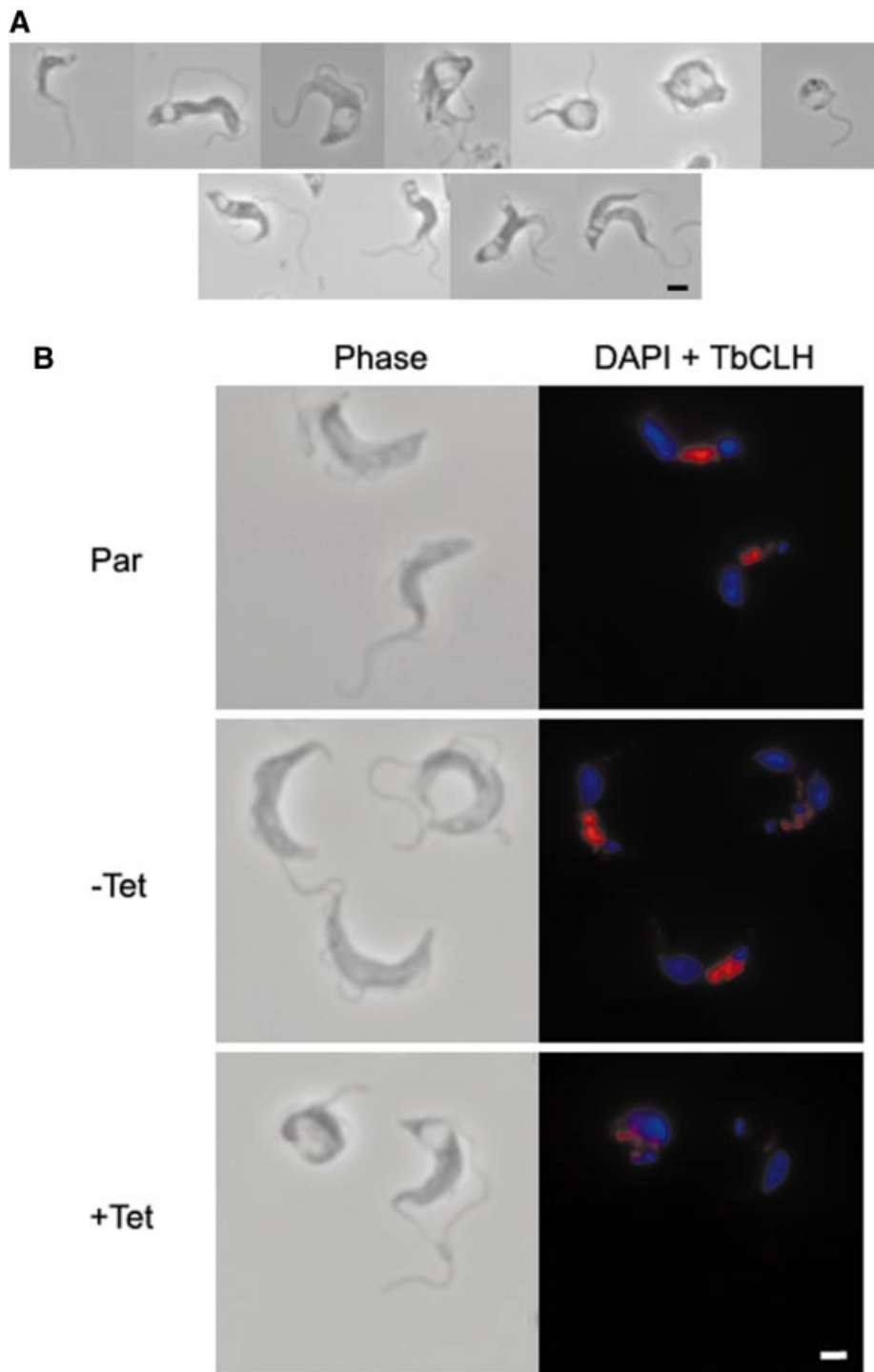
Fig. 1. Depletion of clathrin heavy chain leads to BigEye morphology. (**A**) Gallery of images from cultures expressing clathrin RNAi. The top line shows interphase cells with increased abnormality running from left to right. The majority of cells in early cultures correspond to the four leftmost images, whilst more severe phenotypes, as shown on the right, emerge and increase in prevalence in older cultures. The bottom line shows examples of mitotic cells exhibiting BigEye phenotype. In this case, more than one vacuole is present, and these are frequently of very different sizes (BigEye/LittleEye cells). Scale bar: 2 μm. (**B**) Immunofluorescence analysis demonstrates knockdown of clathrin expression following induction in bloodstream form (BSF) cells. Left, phase-contrast image; right, DAPI (blue) and anti-TbCLH stain (red). Par, BSF 90-13 parental cells; BSFp2T7[Ti]CLH, RNAi cells uninduced (–Tet) and induced (+Tet). Scale bar: 2 μm.

2001), sequences corresponding to caveolin are absent from the genome.

Endocytic mechanisms in *T.brucei* appear to have a role in immune evasion, as well as in normal cellular functions (Morgan *et al*., 2002a,b), and underlie the high level of endocytic activity in the bloodstream form (BSF). Trypanosomes are efficiently lysed by antibody-directed mechanisms if antibody is allowed to remain at the cell surface. Critically, antibody bound to the highly abundant GPI-anchored variant surface glycoprotein (VSG) can be
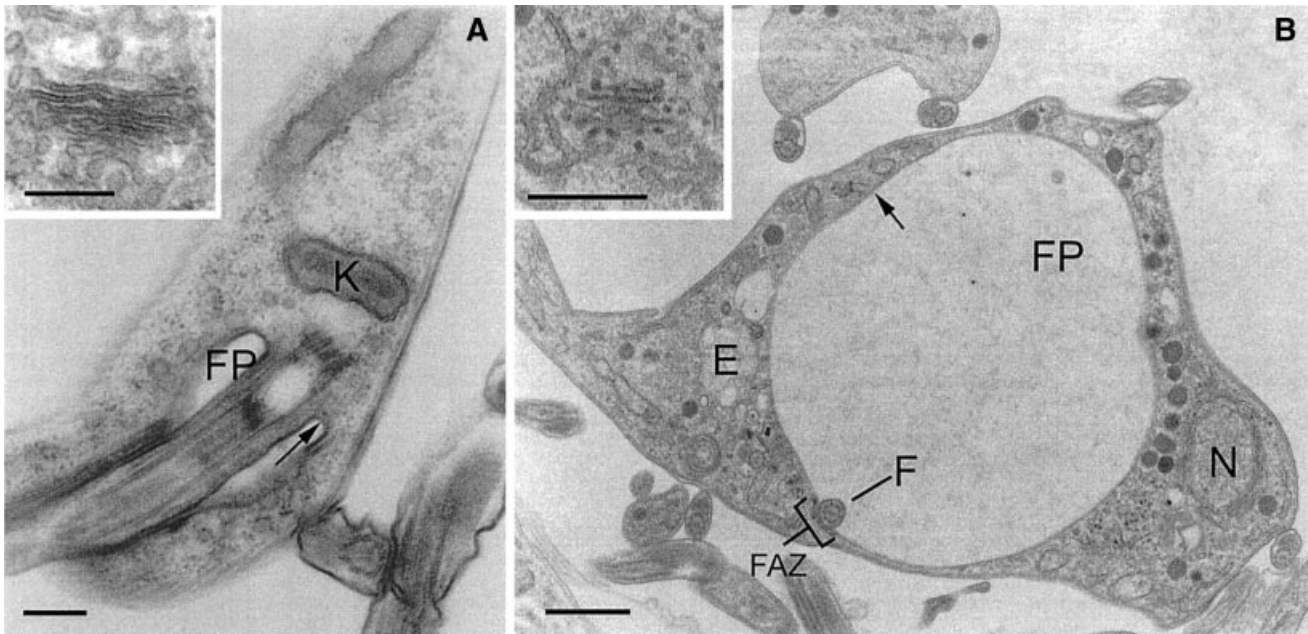
Fig. 2. BigEye is due to flagellar pocket enlargement. (**A**) Parental cells. The flagellar pocket is comparatively small, with a diameter of ~0.5 μm and a flask shape due to tight association with the flagellum. (**B**) Induced clathrin RNAi cells. The flagellar pocket is enlarged. Other structures, including acidocalcisomes, the nucleus and endosomal membranous structures appear normal. Note also the presence of electron-dense material on either side of the flagellum where it contacts the pocket membrane, suggesting the structures responsible for flagellum/flagellar pocket association are still present in this cell. In both (A) and (B), the inset shows a Golgi complex. For both the parental and induced cell lines, the Golgi profile appears normal. E, endosome; F, flagellum; FP, flagellar pocket; FAZ, flagellar attachment zone; K, kinetoplast; N, nucleus. Arrows indicate the electron-dense variant surface glycoprotein (VSG) coat of the flagellar pocket. Scale bars: (A and A inset) 200 nm, (B) 1 μm and (B inset) 500 nm.

rapidly internalized, degraded and recycled (O'Beirne *et al.*, 1998). This pathway involves transport steps mediated by the trypanosome homologues of Rab5 and Rab11 (Jeffries *et al.*, 2001; Pal *et al.*, 2002, 2003). Importantly, both proteins are developmentally regulated (Jeffries *et al.*, 2001; Pal *et al.*, 2002), suggesting that the endocytic system is activated in the bloodstream stage. Here, the role of clathrin in endocytosis has been addressed by functional depletion using RNA interference (RNAi).

Results

Clathrin heavy chain expression is essential in trypanosomes

We expressed double-stranded RNA from the p2T7^{Ti} plasmid corresponding to a portion of the TbCLH open reading frame in BSF and procyclic culture form (PCF) cell lines engineered for inducible expression (LaCount *et al.*, 2000). In both life stages examined, a rapid and severe phenotype was observed, which correlated with decreased expression of the clathrin heavy chain protein (see Supplementary figure 1B available at *The EMBO Journal* Online). In the case of BSF cells, growth ceased very rapidly following induction (within 16 h) and growth cessation continued for about 4 days (see Supplementary figure 1A). After this period, loss of expression of RNAi led to recovery of growth plus re-expression of the clathrin protein. This phenomenon has been observed previously by several workers and is a general feature of RNAi in trypanosomes (Wang *et al.*, 2000).

Decrease of clathrin expression results in 'BigEye' phenotype

Rapidly following induction in BSF cells, a phase light structure was observed in some cells at the posterior end (Figure 1). This structure increased in volume with time, and the proportion of cells exhibiting the abnormal structure was greater after more prolonged induction periods. Eventually, the structure became so large as to fill a major proportion of the cell volume, such that cells became grossly distorted. As the emergence of the structure resembled an eye socket in some examples, we designated this phenotype 'BigEye'.

In the BSF cultures, expression of TbCLH was never completely lost (see Supplementary figure 1B), most likely due to the asynchronous nature of the RNAi system, and was investigated further by immunofluorescence (Figure 1B). The severity of the BigEye morphology correlated well with residual clathrin expression; the examples shown illustrate that low levels of clathrin may be detected in some cells displaying a strong BigEye phenotype (Figure 1B). Hence, it is likely that cells progress through to death rapidly following loss of clathrin expression, and therefore true clathrin-negative cells are a small minority within the population. Importantly, a significant proportion of induced cells were clearly undergoing mitosis (Figure 1, bottom); therefore, depletion of clathrin heavy chain did not prevent mitosis *per se*. Furthermore, in cells undergoing cytokinesis, two posterior structures were present, and these structures were of different sizes (as the larger structure was designated 'BigEye', the smaller structure was designated
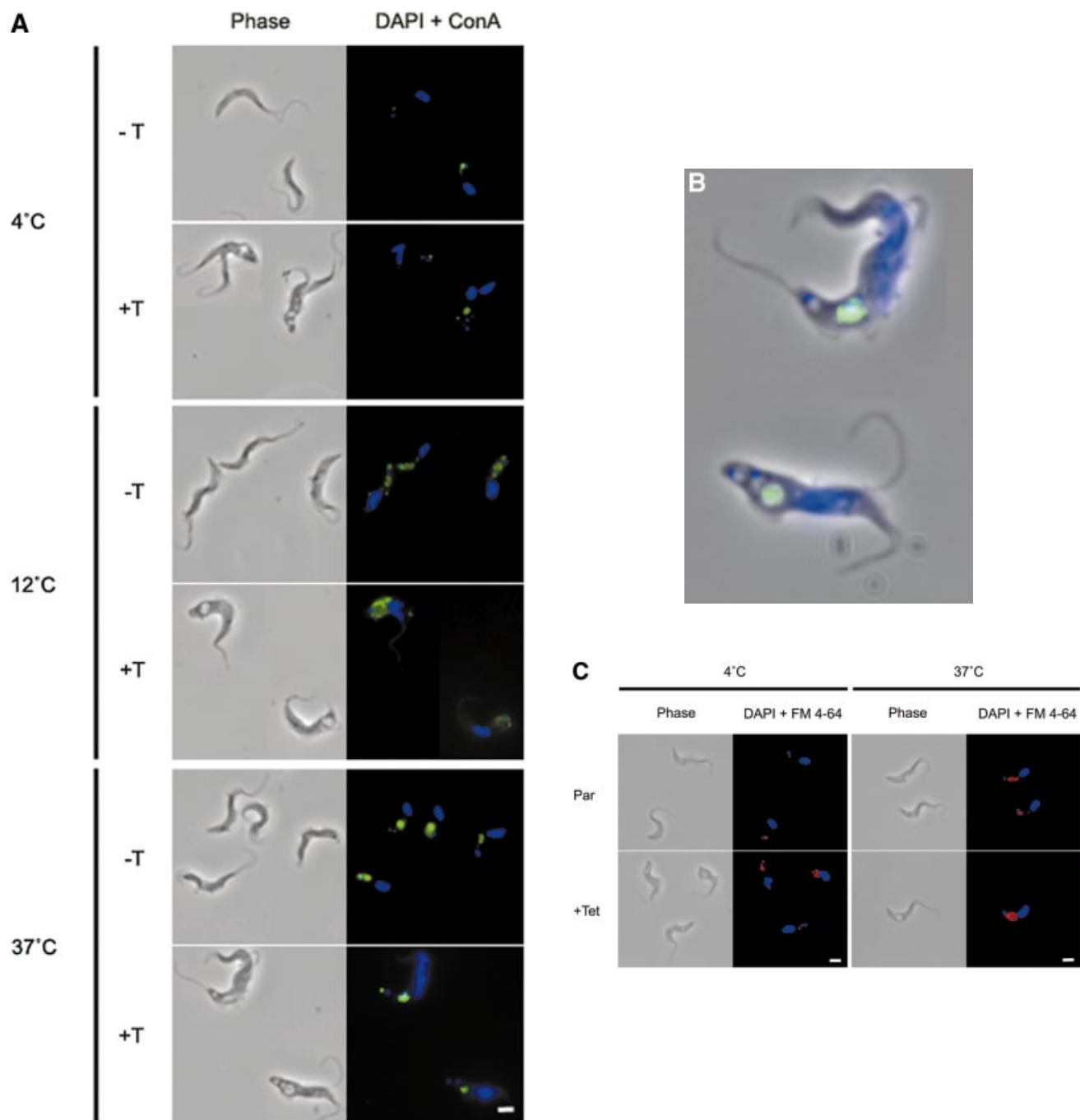
Fig. 3. Endocytosis is perturbed in BigEye cells. (**A**) In uninduced TbCLH RNAi cells at 4°C, lectin concanavalin A (Con A) is retained at the flagellar pocket, at 12°C the lectin is internalized to the endocytic system and at 37°C the lectin is delivered to the terminal lysosome. Induced cells demonstrate a severe defect in uptake. At 37°C, the lectin remains associated with the flagellar pocket. (**B**) Enlarged image of induced bloodstream form (BSF) clathrin RNAi cells (from A), showing that Con A is localized to the enlarged flagellar pocket at 37°C. (**C**) At 4°C, FM 4-64 accumulates in the flagellar pocket in both the parental and induced clathrin RNAi cell line. Note that the staining appears rather more extensive in the RNAi cells due to the enlargement of the pocket. At 37°C, the fluorophore has been internalized in the parental cells, but remains associated with the enlarged pocket structure in the RNAi cell line. (A) Left, phase; right, DAPI (DNA) in blue, lectin in green. (C) Left, phase; right, DAPI (DNA) in blue, FM 4-64 in red. Scale bar: 2 μm. Par, BSF 90-13 parental cells; –Tet, uninduced BSFp2T7^{Ti}CLH cells; +Tet, BSFp2T7^{Ti}CLH cells induced for 16 h.

'LittleEye'). In the vast majority of BigEye cells, the flagellum became detached from the cell body, and many cells had multiple flagellae. In late stage cultures, large numbers of free flagella accumulated, suggesting that the flagellum persists during cellular disintegration.

The BigEye structure is the flagellar pocket
Electron microscopy (EM) demonstrated clearly that the BigEye phenotype was the result of a massively enlarged flagellar pocket (Figure 2). In wild-type cells, this structure is a small flask-shaped structure, but in RNAi cells the
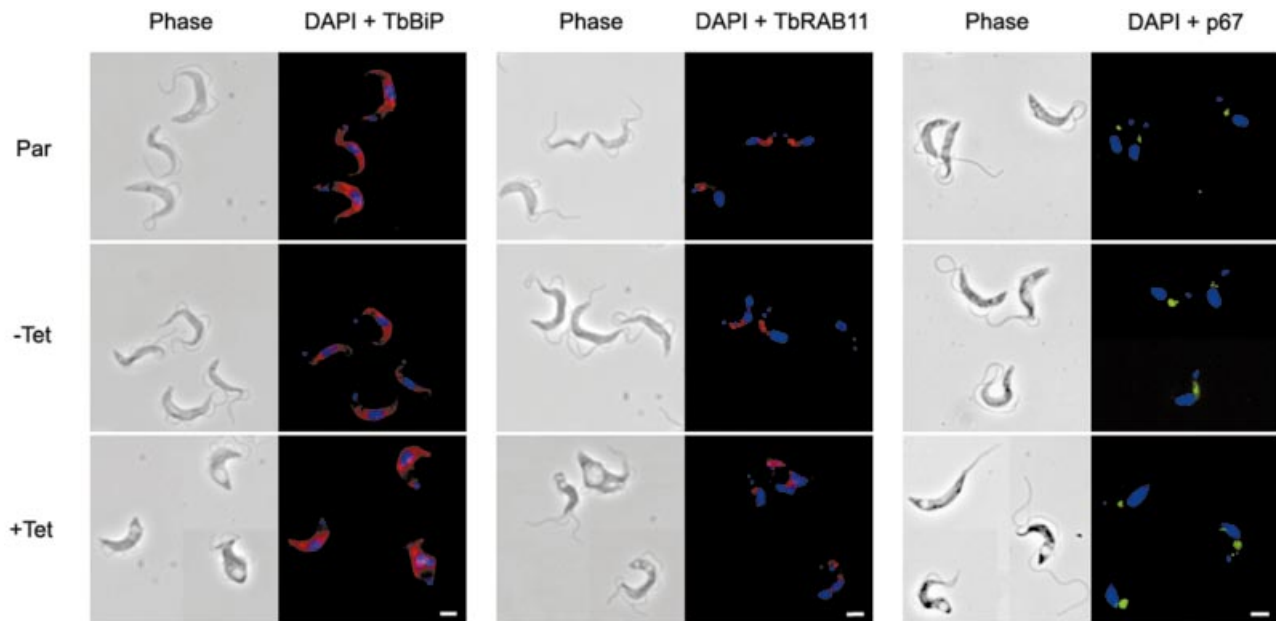
Fig. 4. Preservation of normal morphology of internal membrane structures in BigEye cells. Immunofluorescence analysis for endoplasmic reticulum (TbBiP), recycling endosome (TbRAB11) and lysosomal (p67) proteins. Top, the parental BSF 90-13 cells (Par); middle, uninduced bloodstream form (BSF) RNAi line (–Tet); and bottom, induced (+Tet). Induction is confirmed by the presence of the BigEye. The distribution of marker proteins is unaltered between cell lines. Left, phase; right, DAPI (DNA) in blue, TbBiP or TbRAB11 in red, p67 in green. Scale bar: 2 μm.

pocket became enlarged and filled a substantial proportion of the cell volume. The designation as the flagellar pocket was made by the presence of an electron-dense VSG coat on the membrane, the inclusion of the glycan-rich matrix within the pocket lumen and the presence of the flagellum, bound to the membrane via a visible flagellum attachment zone. Critically, other membranous structures in moderate BigEye cells were unaffected; for example, the Golgi stacks remain with normal morphology (Figure 2). At later times, more extensive disruption of internal membranes was observed, including fragmentation of the nuclear envelope (data not shown). However, these changes are interpreted as arising from toxic effects of clathrin depletion. Enlargement of the flagellar pocket indicates that a severe imbalance in membrane transport occurred, and most likely that endocytosis has been compromised while exocytosis continues. This manifestation of phenotype is radically different from that reported in a vertebrate clathrin knockout study (Wettey *et al.*, 2002) and most likely results from several unusual aspects of the trypanosome system.

Identification of the BigEye vacuole as the flagellar pocket also explained the origin of BigEye/LittleEye mitotic cells. The BigEye is the original flagellar pocket, whereas the LittleEye is most probably the daughter pocket, the size difference being due to the shorter period of time that the second pocket has been present. Importantly, the emergence of an enlarged pocket indicates that the daughter structure becomes active for exocytosis prior to completion of cytokinesis.

BigEye cells are defective in endocytosis

An assay to monitor exocytosis of VSG, which accounts for ~90% of cell surface protein, indicated that export of this protein was unaffected (see Supplementary data and Supplementary figure 2). Assays of several modes of endocytosis were used to assess the ability of BigEye cells to carry out internalization. Trypanosomes actively endocytose the mannose-binding lectin concanavalin A (Con A), an excellent marker for membrane-bound endocytic activity (Brickman *et al.*, 1995). At 4°C, Con A is restricted to the flagellar pocket, whereas at 12°C the lectin penetrates deeper into the cell, and localizes to the TbRAB5A endosome, or collecting tubules (Jeffries *et al.*, 2001). At 37°C, the lectin is endocytosed into the lysosome (see Supplementary figure 4A). Essentially identical staining was obtained in uniduced cells, but Con A was not transported correctly in induced cells (Figure 3A). At 4°C, Con A marked the flagellar pocket, but at 12°C and 37°C most of the lectin remained associated with the flagellar pocket, indicating a decrease in Con A endocytosis. Additional co-staining for both the flagellar pocket and markers for endocytic compartments confirmed a gross defect in endocytosis (see Supplementary data and Supplementary figure 4B and C). A similar accumulation of material in the flagellar pocket was also obtained with anti-VSG antibody capping experiments (see Supplementary data and Supplementary figure 4D).

The effect of clathrin depletion on bulk lipid endocytosis was also evaluated using the fluorophore *N*-(3-triethylammoniumpropyl)-4-{6-[4-(diethylamino)phenyl]-hexatrienyl} pyridinium dibromide (FM 4-64). Again, at 4°C, most of this label is found in the flagellar pocket in parental cells, but at 37°C the fluorophore is efficiently endocytosed to internal membrane compartments. In contrast, in the BigEye cells, FM 4-64 stains a more extensive structure at 4°C, consistent with the enlarged flagellar pocket, and at 37°C the stain remains associated with this membrane (Figure 3C). Hence, a general lipid
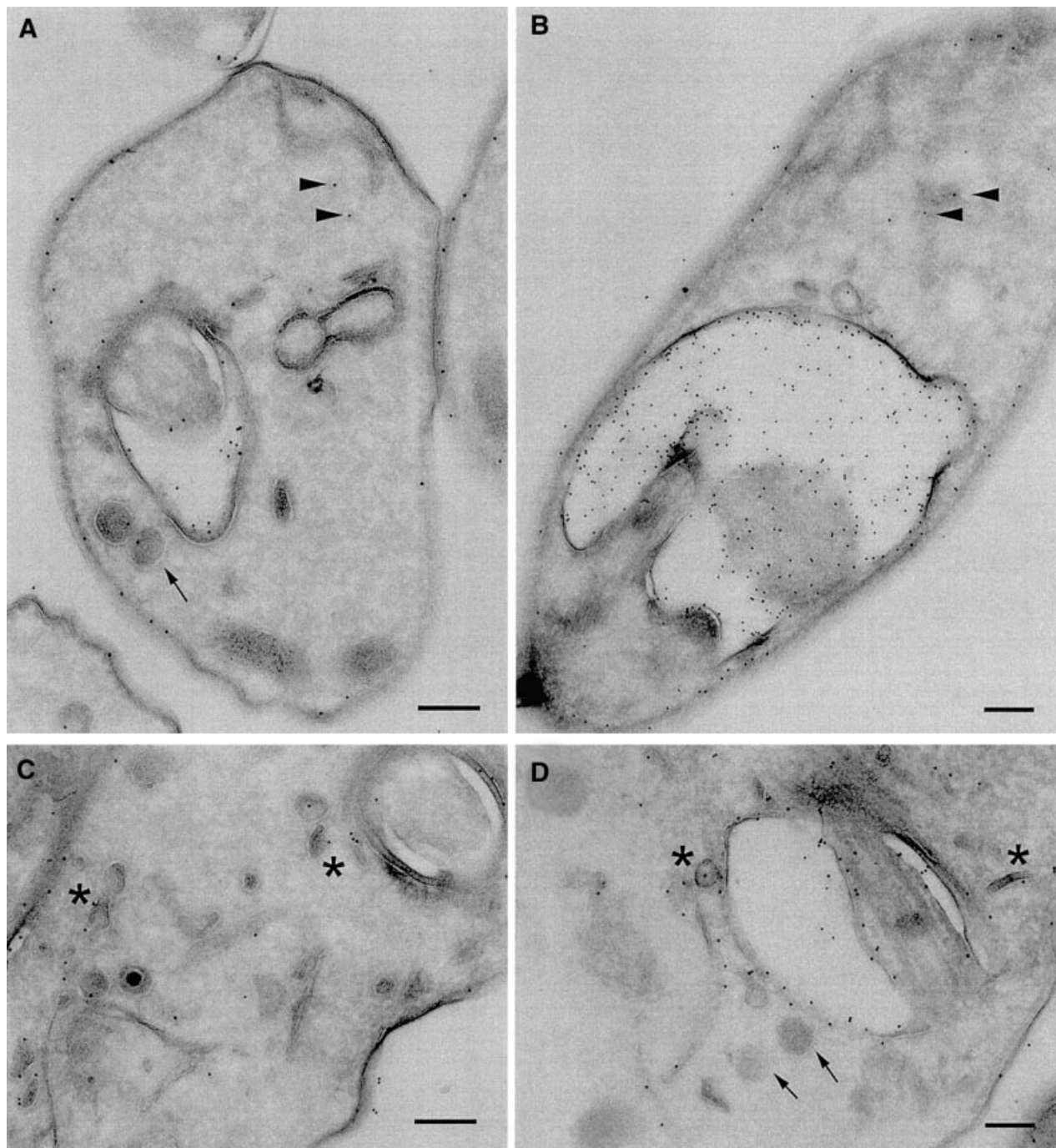
Fig. 5. Variant surface glycoprotein location in BigEye cells. CryoimmunoEM images of parental (**A** and **C**) and clathrin-depleted cells (**B** and **D**). Variant surface glycoprotein (VSG) is observed on the plasma membrane, within the flagellar pocket and over a number of internal structures, tentatively assigned as endoplasmic reticulum (arrowheads) and TbRAB11 recycling endosomes (arrows), based on previous studies (Grunfelder *et al.*, 2002, 2003). In the BigEye cells, VSG is also seen with similar distribution on the plasma membrane, endoplasmic reticulum and in recycling endosome figures. Hence, VSG remains associated with TbRAB11 transport intermediates, and these structures retain normal morphology. Scale bar: 200 nm.

probe also exhibits defective endocytosis. These data indicate an extreme blockade to endocytosis of Con A receptors (VSG and other glycoproteins), anti-VSG antibody and lipid membranes.

Other membrane compartments are unaffected in BigEye cells

The dramatic decrease in endocytosis and the morphological distortion of the BigEye cells could have a profound effect on structures not sampled by EM. BigEye cells were analysed for the distribution of endoplasmic reticulum (ER), endosomes and the lysosome by staining with antibodies against TbBiP, TbRAB11 and p67, respectively (Bangs *et al.*, 1993; Jeffries *et al.*, 2001; Alexander *et al.*, 2002) (Figure 4). The distributions of all of these markers were unchanged in BigEye cells, suggesting that these structures were essentially unaltered in BSF parasites depleted of clathrin.
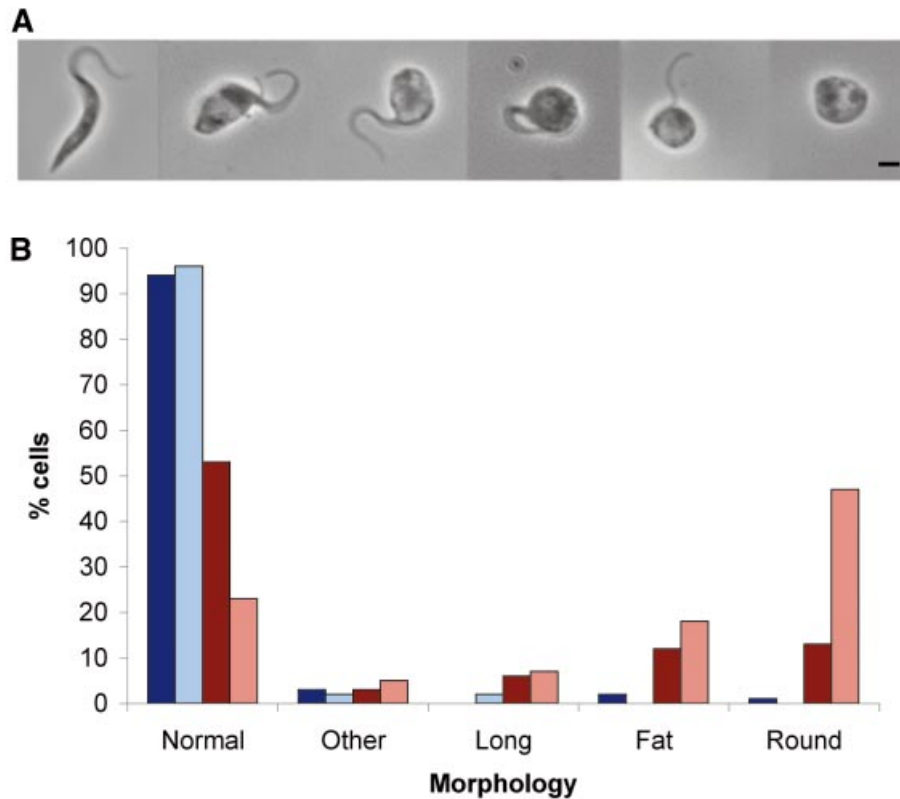
Fig. 6. Depletion of clathrin heavy chain in procyclic culture form (PCF) cells leads to a rounded morphology. (**A**) Gallery of phase images from PCF cultures expressing clathrin RNAi. The leftmost image shows the 'normal' PCF phenotype, the next two images show the 'fat' phenotype, and the three images on the right show the 'round' phenotype. (**B**) Incidence of aberrant cell morphologies in induced PCF clathrin RNAi cell cultures. Blue bars, uninduced PCFp2T7^{Ti}CLH cells cultured for 48 h (dark blue) or 72 h (pale blue); red bars, induced PCFp2T7^{Ti}CLH cultures at 48 h (dark red) or 72 h (pale red). Morphologies were defined as follows: normal, average cell body length 15 μm, average width 1.54 μm; long, cell body length >20 μm, average cell body length 23.3 μm, average width 1.54 μm; fat, enlarged posterior of the cell, average cell body length 8.55 μm, average width 3.07 μm; round, cell body completely rounded up, with detached or no visible flagellum, average cell body length 4.66 μm, average width 4.26 μm; other, all other abnormal forms.

Furthermore, we investigated the distribution of VSG and endosome structures by cryoimmunoEM. Parental cells and induced clathrin RNAi cells were sectioned and stained with anti-VSG 221 antibodies at a low concentration (Figure 5). In the parental cells, gold particles decorated the plasma membrane, the flagellar pocket membrane and a number of intracellular structures (Figure 5A and C), including tubular structures most likely ER, plus highly characteristic smaller electron-dense structures that appear as small tubules or discs described elsewhere as TbRAB11 recycling endosomes (Grunfelder *et al.*, 2003). These data, together with the exocytosis assay in the Supplementary data, indicate that VSG can be detected at the surface, in the recycling system and, less prominently, in the biosynthetic apparatus (Grunfelder *et al.*, 2003).

When BigEye cells were analysed, a broadly similar distribution of gold particles was obtained; significantly, despite a similar gold particle density being recovered on the plasma membrane, a much increased concentration of VSG was observed in the flagellar pocket and, in particular, in the lumen (Figure 5B and D). The origin of the luminal VSG is unclear, but it may have been shed from the membrane (Geuskens *et al.*, 2000); the absence of endocytosis in these cells would suggest that the shedding phenomenon does not involve the recycling system. Gold

particles were detected over ER membrane and associated with TbRAB11 endosomes (Figure 5D). These data indicate that recycling compartments are still present in the BigEye cells, and therefore their integrity does not depend on continuous endocytosis.

Intracellular compartments are more distorted in procyclic clathrin RNAi cells than in the BSF

Several major differences in the endocytic routing of proteins have been reported between procyclic and bloodstream stage *T.brucei*. In contrast to the distinct BigEye morphology of induced BSF clathrin RNAi cells, a range of distinct morphologies were observed in PCF clathrin RNAi cultures. To determine which morphology was associated with the loss of TbCLH expression, the incidence of each phenotype was scored by light microscopy of fixed cells from cultures induced for 24, 48 or 72 h in comparison with uninduced and parental cell cultures. Ninety-seven percent of both uninduced and induced cells at 24 h growth showed morphology essentially indistinguishable from parental cultures (data not shown). The number of normal cells in induced cultures dropped to 53% after 48 h and to 23% by 72 h (Figure 6B). As the number of normal cells decreased, the number of 'fat' and 'round' cells increased. The fat cells are probably precursors of the round cells (Figure 6A), suggesting that
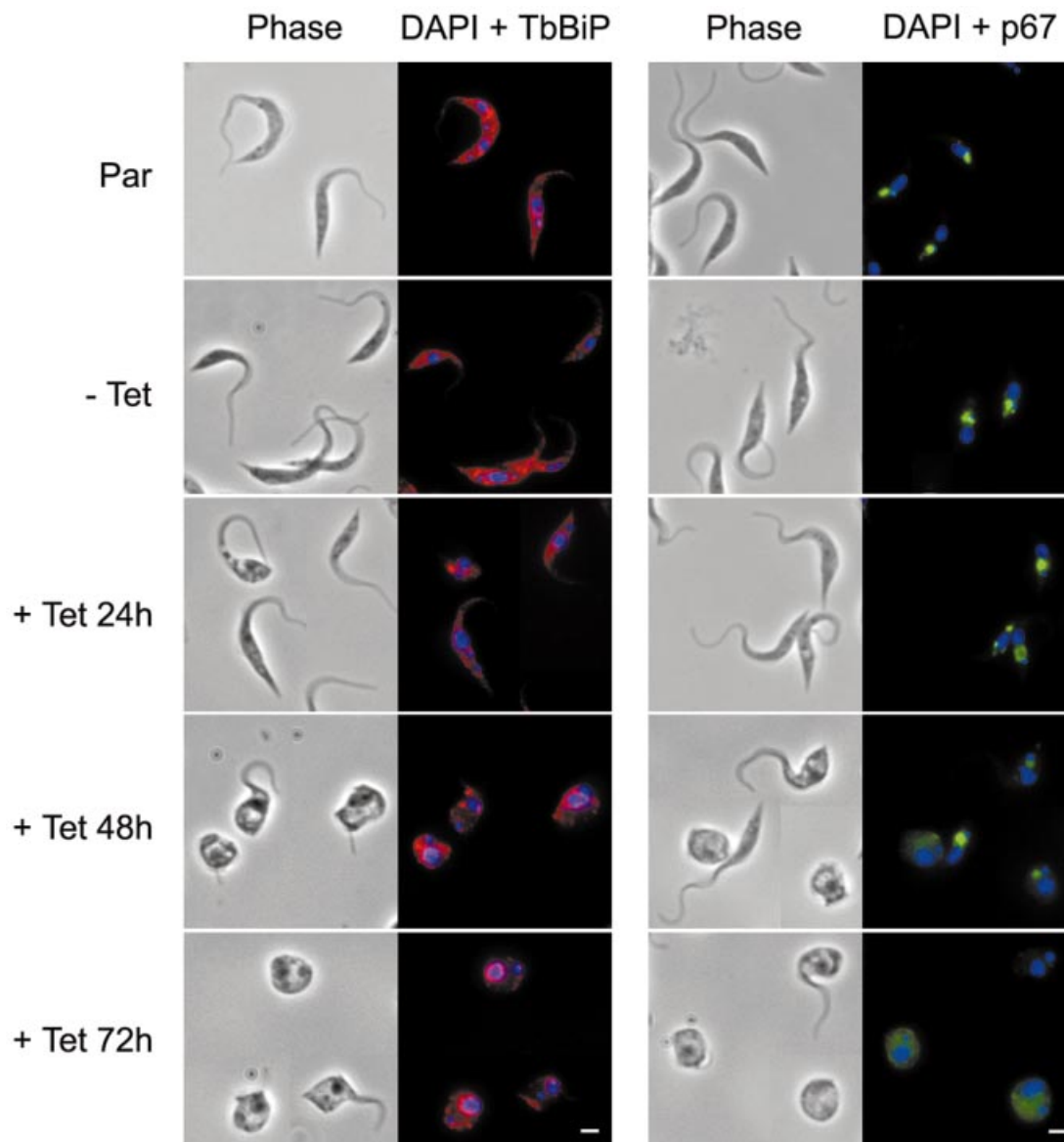
Fig. 7. Alteration of lysosomal protein targeting in procyclic culture form (PCF) BigEye cells. Clathrin RNAi cells were stained following 24, 48 and 72 h of induction as indicated. For TbBiP a disorganization was observed, suggesting that the endoplasmic reticulum has become deformed. In addition, the localization of p67 was altered, so that at 48 h the stain was less intense and defocused, and at 72 h this was more extreme with a major loss of integrity. Left image of each set, phase; right image, DAPI (DNA) in blue, TbBiP in red, p67 in green. Scale bar: 2 μm. Par, PCF 29-13 parental cells; –Tet, uninduced PCF 29-13p2T7[Ti]CLH cells; +Tet, PCF29-13p2T7[Ti]CLH cells induced for indicated time periods.

loss of TbCLH expression results in gradual rounding up of the cell and detachment or loss of the flagellum. By EM, these cells exhibited a most remarkable phenotype, completely distinct from the BSF RNAi cells. Massive numbers of vesicles, of ~50–400 nm diameter, were observed to fill the cytoplasm (Figure 8A and B), but there were no manifest effects on the nucleus, mitochondrion or kinetoplast. The PCF clathrin RNAi cells were also distorted, being rounded up; this morphology is most likely a result of internal pressure due to the presence of excess membrane accumulating within the cytoplasm. Some of the vesicles contained electron-dense matrix material, which may indicate a flagellar pocket origin. Major perturbation to the *trans*-Golgi complex was observed in many cells (Figure 8C and D). Even a comparatively normal cell (Figure 8A) possesses a

distorted *trans*-Golgi stack. A similar phenotype was obtained in clathrin-deficient *Saccharmoyces cerevisiae*, where the accumulated vesicles were assigned as Berkeley bodies, post-Golgi transport intermediates (Payne *et al.*, 1987). Clearly, these data indicate that the main effect in the PCF is not flagellar pocket enlargement, but an accumulation of transport intermediates within the cytoplasm.

The distributions of selected markers were examined in PCF RNAi cells (Figure 7). A clear alteration in p67 distribution was observed, with the lysosomal localization becoming less clear; at 48 h induction staining of the lysosome decreases in intensity in the 'fat' and 'round' cells and at 72 h the stain was diffuse, suggesting loss of p67 from lysosomal membranes and mislocalization throughout the cell. There was also a clear alteration in
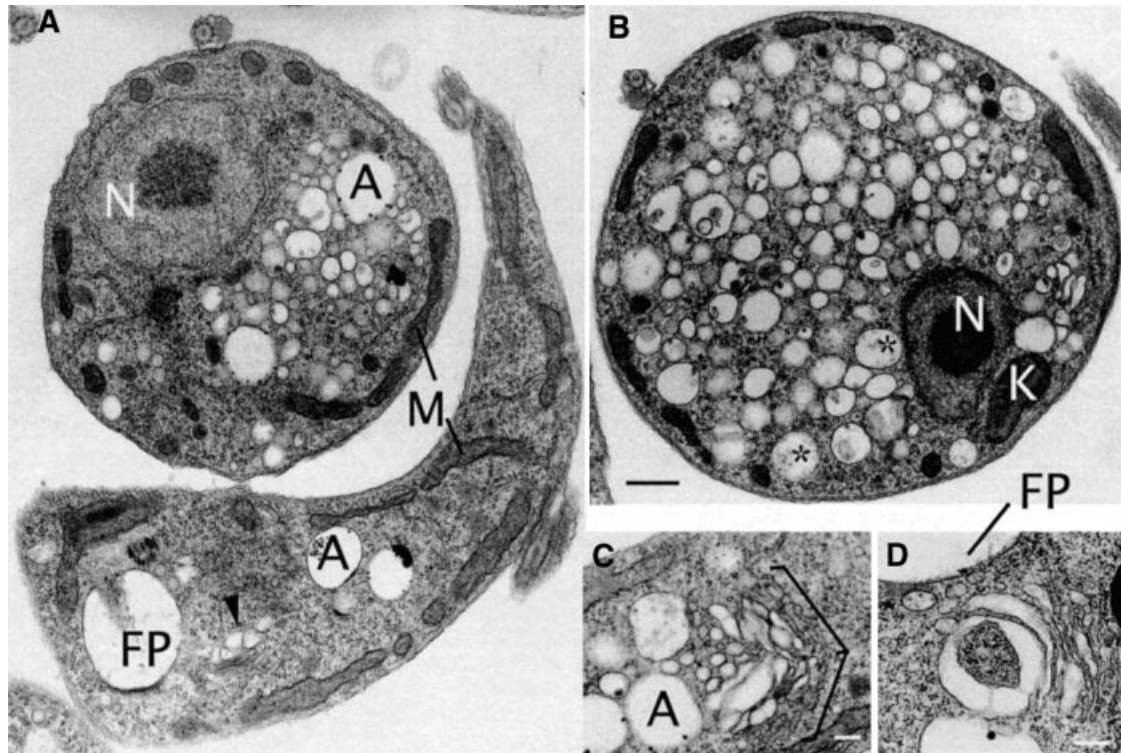
Fig. 8. A distinct ultrastructural defect accompanies TbCLH-depletion in procyclic culture form (PCF) trypanosomes. Electron micrographs of PCF cells following 48 h induction of clathrin dsRNA. (**A**) Two cells exhibiting normal (bottom) and abnormal (top) phenotypes. The major effects of clathrin double-stranded RNA expression is in the accumulation of vesicular profiles of variable diameter (~50–400 nm) and a rounding up of the cell. Other structures (nucleus, mitochondria, acidocalcisomes) appear normal. (**B**) A more extreme example of a PCF clathrin RNAi cell. The plasma membrane has become smooth, possibly due to increased cytoplasmic pressure. In addition, the nucleus, kinetoplast and mitochondria appear normal. (**C** and **D**) Details of the Golgi region of PCF RNAi cells showing distortions to the *trans*-Golgi cisternae and membranes. The cell in (C) is in early mitosis, as the Golgi stack appears to be undergoing binary fission (Field *et al.*, 2000). A, acidocalcisomes; K, kinetoplast; FP, flagellar pocket; M, mitochondria; N, nucleus; *, vesicles containing electron-dense matrix-like material (possibly FP-derived); arrowhead, distorted *trans*-Golgi. Scale bars: (A and B) 500 nm, (C) 200 nm and (D) 250 nm.

distribution of TbBiP in induced cells. Again, at 48 h TbBiP was concentrated around the nucleus, with almost all TbBiP staining becoming perinuclear in cells induced for 72 h.

Discussion

Clathrin ablation in trypanosomes is lethal, which sets this divergent organism apart from yeast and vertebrates where deletion of the clathrin gene or protein is tolerated (Seeger and Payne, 1992; Wettey *et al.*, 2002). Despite a significant developmental expression profile that correlates with endocytic activity, clathrin expression is required for viability in both life stages (Morgan *et al.*, 2001). In mammals, endocytosis is dispersed across the entire plasma membrane. Endocytosis is extremely rapid in trypanosomes, and more rapid within the flagellar pocket zone than in individual mammalian cells, and hence the phenotype is very severe in the protozoan. Additionally, the trypanosome plasma membrane is tightly anchored to a subpellicular microtubule array, which prevents abnormal addition of membrane to this region; hence, any membrane overflow must be retained within the flagellar pocket. The physical stress induced by the addition of membrane to the flagellar pocket may also be the major cause of cellular mortality, probably due to compression of the cytoplasm

and the presence of a large expanse of non-supported membrane in the pocket.

In the BSF, loss of clathrin expression led to a massive enlargement of the flagellar pocket. Moreover, all evidence, from multiple assays for endocytosis, indicated that the levels of endocytic activity were dramatically compromised in these cells, but at the same time exocytosis of VSG appears to be unimpaired. Despite this, both ultrastructural analysis and immunofluorescence using established marker proteins for the ER (TbBiP), recycling endosomes (TbRAB11) and the lysosome (p67) (Bangs *et al.*, 1993; Jeffries *et al.*, 2001; Alexander *et al.*, 2002) indicated that other membrane compartments were essentially unaffected, and hence the flagellar pocket enlargement represents the primary phenotype in this life stage. A comparatively low level of clathrin heavy chain immunoreactivity on Golgi complex membranes is consistent with this interpretation (Morgan *et al.*, 2001). The connection between the subpellicular array and the plasma membrane is clearly maintained, as demonstrated by ultrastructural analysis.

The lethality of clathrin heavy chain ablation in the BSFs had a rapid onset. The appearance of the enlarged flagellar pocket correlated with residual expression of the clathrin protein; cells possessing the largest flagellar pockets were devoid of clathrin immunoreactivity, whereas trypanosomes retaining clathrin expression had

a smaller flagellar pocket. The rapidity of the onset of the BigEye phenotype, where significant numbers of abnormal cells were observable after a 10 h induction period, indicates a rapid turnover for clathrin in this stage. The BigEye cells were observed to be highly fragile, and even low speed centrifugation resulted in lysis of the majority of BigEye cells (data not shown). Taken together, these data suggest that the mechanism of cell death in these cells is due to mechanical failure, most likely membrane rupture due to extreme pressure on the cell as the cytoplasm becomes compressed by the enlarging pocket. However, it is of significant interest that the pocket retained a near-spherical configuration, which may suggest the presence of luminal or membrane-associated components responsible for providing a compensatory pressure to oppose that from the cytoplasm. One possible candidate would be the gel-like glycan-rich matrix within the pocket lumen.

Significantly, the severity of the phenotype also brought to light a significant asynchrony in the loss of clathrin from individual cells within an induced culture. After 16 h, cells with normally sized flagellar pockets were present alongside cells fully devoid of the clathrin heavy chain, but the proportion of cells exhibiting the most extreme phenotype increased in the population over time, indicating that those cells at earlier times with residual clathrin expression were not simply RNAi deficient. In fact, a very small number of cells appeared to survive the RNAi, and these grew out after several days, re-expressed clathrin and had a normal morphology.

In contrast to the BSF, the lethality of loss of clathrin in the procyclic stage exhibited a slower onset, with a clear loss of viability from 48 h. As the PCF has a greatly reduced rate of endocytosis (Pal *et al*., 2002), this was not an unexpected finding. At the light level, the PCF cells became round, and ultrastructural analysis indicated that the flagellar pocket was not enlarged, but rather that a severe accumulation of transport vesicles had taken place, most likely equivalent to Berkeley bodies of *Saccharomyces* (Payne *et al*., 1987). The alteration of p67 staining in these cells suggests a sorting defect, the diffuse staining resulting from mislocalization of this membrane to the multiple vesicles present in these cells. The perinuclear TbBiP localization may also result from the presence of multiple transport vesicles, which fill the PCF clathrin RNAi cells, causing the ER to be deformed and restricted to the perinuclear region rather than spreading throughout the cell.

The most likely interpretation of the PCF phenotype is that transport vesicles are produced but are unable to fuse with the target membrane. There is strong evidence for multiple roles for clathrin in endosomal sorting, post-Golgi transport and trafficking to the lysosome in higher eukaryotes (Boehm and Bonifacino, 2002), and recent data suggests a similar role in trypanosomes (Grunfelder *et al*., 2003). The possibility that PCF cell death is due to nutrient starvation was investigated by culturing PCFs in serum-free medium; these cells did not exhibit the same morphological abnormalities as seen by the clathrin RNAi, and they survived for significantly longer. Therefore, it is likely that cell death in the PCF is not due to the inability to endocytose essential nutrients.

Broadly similar sorting mechanisms probably exist in both the PCF and the BSF (Morgan *et al*., 2002a,b), so why do transport intermediates accumulate in the PCF and not in the BSF? Most likely, the extreme level of endocytic activity in the BSF has the consequence that, as soon as clathrin levels become significantly depleted, the flagellar pocket enlarges and rapid cell death occurs via plasma membrane rupture. Even in induced BSF cultures, significant accumulation of intracellular vesicles was not observed. Hence, although clathrin may well mediate similar pathways in both PCF and BSF, the relative flux through the endocytic and post-Golgi/recycling/sorting pathways may well be radically different, giving rise to the stage-specific phenotypes. Specifically, the major activity is endocytosis in BSF and post-Golgi transport in PCF.

Perhaps most importantly, the absence of detectable endocytosis in the clathrin RNAi cells indicates that GPI-anchored proteins in this organism must be endocytosed via a clathrin-mediated mechanism. This conclusion is further strengthened by ultrastructural evidence demonstrating VSG in clathrin-coated pits and vesicles (Grunfelder *et al*., 2003). It is likely, given the high concentration of VSG on surface membranes, that little, if any, cargo selection can take place at the point of initial endocytosis, a proposal that is further supported by the absence of trypanosome AP-2 complex subunits in the databases (Morgan *et al*., 2002b). These observations also suggest that clathrin-mediated endocytosis is ancient (or emerged earlier than other forms of endocytosis), as caveolin homologues are also absent from the trypanosome genome, suggesting that this latter system is a more recent addition to the endocytic repertoire and may have evolved to deal with a more complex cell surface architecture, where GPI anchors are no longer the dominant form of protein membrane attachment and where more effective protein sorting mechanisms are required. Other vesicle coat systems have also been described in trypanosomes, including direct demonstration of COP I (Maier *et al*., 2001), while elements of the COP II system are present in the databases (M.C.Field, unpublished data), but the lethality of clathrin ablation suggests a fundamental lack of flexibility in the trypanosome endocytic pathway.

Materials and methods

Trypanosome growth and induction of RNAi

PCF 29-13 and BSF 90-13 *T.brucei* Lister 427 strain cell lines were gifts from Elizabeth Wirtz and George Cross (Rockerfeller University) (Wirtz *et al*., 1999). Cell lines were grown in SDM79 or HMI9 media, supplemented with 10% heat inactivated fetal bovine serum, as appropriate (Field *et al*., 1998), and cultured in the continuous presence of 25 µg/ml G418 and 25 µg/ml hygromycin (PCFs) or 2 µg/ml G418 and 5 µg/ml hygromycin (BSFs). Following transfection, expression of double-stranded RNA was induced by the addition of tetracycline at 1 µg/ml.

RNAi plasmid construction and transfection

To generate the plasmid p2T7^{Ti}CLH, a 521 bp fragment of the *TbCLH* gene was PCR amplified from *T.brucei* 427 strain genomic DNA using the primers 5′-CCCAAGC TTCTAGAGATTAACCTG-3′ and 5′-CCT-CTCGAGTTCCTGCACCTGCCC-3′, which contain restriction sites for *Hin*dIII and *Xho*I, respectively. An extra *Xho*I site was generated in this fragment by PCR, causing a 127 bp fragment to be lost from the 3′ end on subsequent digestion. However, the remaining 394 bp fragment of the *TbCLH* gene was subcloned via pBluescript II SK as a *Bam*HI–*Xho*I fragment into the tetracycline inducible RNAi vector p2T7^{Ti} (a gift from

Douglas LaCount and John Donelson) (LaCount *et al*., 2002) yielding p2T7^Ti^CLH.

For transfection into the PCF 29-13 cell lines, 20 µg of *Not*I linearized p2T7^Ti^CLH plasmid was added to 2×10^7 log phase cells in a total volume of 0.45 ml of Opti-MEM (Invitrogen). The sample was mixed, then transferred to a pre-cooled 2 mm gap electrocuvette (Bio-Rad) and chilled on ice for 5 min prior to electroporation (Bio-Rad Gene Pulser II electroporator, 1.5 kV, 25 µF). Immediately following electroporation, the cells were transferred into 10 ml of SDM79/10% HI-FBS containing 25 µg/ml G418 and 25 µg/ml hygromycin and left to recover at 27°C overnight. Approximately 16 h following electroporation, phleomycin was added at 2.5 µg/ml to select for transformants.

The BSF 90-13 cell line was transfected with 5–10 µg of *Not*I linearized p2T7^Ti^CLH using 2.5×10^7 log phase cells per transfection. Cells were resuspended in 0.4 ml of pre-warmed cytomix (van den Hoff *et al*., 1992) (37°C) and mixed with the DNA in 50 µl of cytomix before being transferred to a 2 mm Bio-Rad cuvette (at ambient temperature). The sample was electroporated at 1.4 kV, 25 µF, and the cells transferred into 48 ml of HMI9 containing 2 µg/ml G418 and 5 µg/ml hygromycin. The cells were left to recover for 6 h at 37°C/5% CO$_2$ prior to the addition of phleomycin at 2.5 µg/ml for selection. The cells were then transferred to a 24-well tissue culture plate (2 ml per well) and left for drug-resistant cells to recover. Clonal cell lines were obtained by serial dilution.

Protein electophoresis and western blotting

For protein extraction, mid-log phase cells were harvested, washed in PBS (Sigma) then resuspended in boiling SDS–polyacrylamide sample buffer at a concentration of 1×10^6 cell equivalents per microlitre. Samples were electrophoresed on 10% SDS–PAGE minigels gels at 1×10^7 cell equivalents per lane and then transferred to Hybond-ECL nitrocellulose membrane (Amersham Pharmacia Biotech) by wet blot using transfer buffer [192 mM glycine, 25 mM Tris, 20% (v/v) methanol]. Transfer and equivalence of loading were checked by staining the membrane with Ponceau S solution (Sigma) prior to blocking for 1 h at room temperature in blocking solution [TBS (24.8 mM Tris, 137 mM NaCl, 2.7 mM KCl)/0.05% Tween-20/3% dried milk]. Membranes were incubated for at least 1 h at room temperature with primary antibody at the appropriate dilution in blocking solution, washed 4×5 min in TBS/0.05% Tween-20, then incubated for a further hour with horseradish peroxidase goat anti-rabbit conjugate (Sigma). After washing, bound antibodies were detected by reaction with luminol and visualized by exposure to X-ray film. Both primary antibodies, rabbit anti-TbCLH Ab (Morgan *et al*., 2001) and rabbit anti-TbBiP Ab (a gift from James Bangs, Madison), were diluted 1:1000 for use in western blots.

Immunofluorescence microscopy

Indirect immunofluorescence microscopy was performed on BSF and PCF trypomastigotes harvested at log phase growth. BSF cells were washed in VPBS (136.9 mM NaCl, 3 mM KCl, 16 mM Na$_2$HPO$_4$, 3 mM KH$_2$PO$_4$, 45.9 mM sucrose, 10 mM glucose) (Nolan *et al*., 2000) then fixed for 1 h at 4°C in 3% paraformaldehyde (PFA). Fixed cells were adhered to poly-L-lysine-coated polyprep slides (Sigma) for 20 min at room temperature, then permeabilized with 0.1% Triton X-100 (Sigma) in PBS for 10 min. The slides were blocked for 1 h at room temperature in PBS/10% goat serum, then incubated with the primary antibody at the appropriate dilution in PBS/10% goat serum at room temperature for a further hour. Unbound primary antibody was washed off with PBS/0.05% Triton X-100 prior to incubation with secondary antibodies: Cy3-labelled anti-rabbit IgG (Sigma) or Oregon-green-labelled anti-mouse IgG (Molecular Probes), diluted according to manufacturer's instructions. All cells were stained with DAPI at 0.5 µg/ml to visualize the nucleus and kinetoplast.

Essentially the same procedure was used for immunofluorescence microscopy of PCF trypomastigotes, except that these cells were fixed directly in culture with 3.7% formaldehyde for 30 min at room temperature prior to adhesion to the slides. Cells were examined using a Nikon ECLIPSE E600 microscope, and images were captured using a Photometrics CoolSNAP FX camera. Digital images were captured and false coloured using MetaMorph 5.0 software (Universal Imaging Corporation). Figures were assembled from these images using Adobe Photoshop 7.0 (Adobe Systems). Primary antibodies were used at the following dilutions: rabbit anti-TbCLH, 1:500 (Morgan *et al*., 2001); rabbit anti-TbBiP (Bangs *et al*., 1986), 1:1500 and mouse anit-p67, 1:500 (both gifts of James Bangs, Madison); and rabbit anti-TbRAB11, 1:1000 (Jeffries *et al*., 2001).

Uptake assays

To follow receptor-mediated endocytosis, Con A uptake was performed as described previously (Brickman *et al*., 1995), with the following modifications. Each assay was performed using 1×10^7 BSF parasites incubated at the appropriate temperature in 1 ml of serum-free HMI9 supplemented with 1% BSA and containing 5 µg/ml FITC-Con A (Vector Laboratories). Mid-log phase parasites were pre-incubated for 30 min in serum-free HMI9 supplemented with 1% BSA at 4°C, 12°C or 37°C. FITC-Con A was then added to the parasites at a final concentration of 5 µg/ml, and the cells were incubated for a further 30 min at the appropriate temperature. After incubation, the cells were transferred to ice and all subsequent manipulations were performed using pre-chilled buffers, on ice, in the cold room. The parasites were washed once in ice-cold VBPS and then fixed in 3% PFA/VPBS at 4°C for 1 h.

Membrane internalization was monitored by following uptake of FM 4-64 (Molecular Probes). The procedure was carried out at 4°C or 37°C on 5×10^7 cells in 250 µl TES buffer (120 mM NaCl, 5 mM KCl, 3 mM MgSO$_4$, 16 mM Na$_2$HPO$_4$, 5 mM KH$_2$PO$_4$, 30 mM TES, 10 mM glucose, 0.1 mM adenosine pH 7.5). The cells were pre-incubated for 10 min at the appropriate temperature prior to addition of FM 4-64 at a final concentration of 40 µM, followed by incubation for a further 5 min. The cells were then transferred to ice, fixed with 3% PFA/VPBS and mounted as described above.

Electron microscopy

For transmission EM, cells were fixed in suspension by adding chilled 5% glutaraldehyde (TAAB) and 8% PFA (Sigma) in PBS in a 1:1 ratio to the growth medium containing trypanosomes. Cells were fixed on ice for 10 min, centrifuged at 10 000 r.p.m. for 5 min in 2 ml Eppendorf tubes, the supernatant carefully replaced with fresh fixative for a further 50 min without disturbing the pellet, rinsed in 0.1 M sodium cacodylate and post-fixed in 1% osmium tetroxide (TAAB) in the same buffer at room temperature for 1 h. After rinsing, cells were dehydrated in an ethanol series, adding 1% uranyl acetate at the 30% stage, followed by propylene oxide and then embedded in Epon/Araldite 502 (TAAB) and finally polymerized at 60°C for 48 h. Sections were cut on a Leica Ultracut T ultramicrotome at 70 nm using a diamond knife, contrasted with uranyl acetate and lead citrate and examined on a Philips CM100 transmission electron microscope.

For cryosections, cells were fixed in suspension by adding chilled 0.4% glutaraldehyde and 8% PFA in PBS in a 1:1 ratio to the growth medium containing trypanosomes to give final dilutions of 0.2% glutaraldehyde and 4% PFA. Cells were fixed for 10 min on ice, centrifuged and the supernatant replaced for fresh fixative for a further 50 min on ice to fix the pellet. The cells were then rinsed three times in cold PBS over 15 min and then infused with cold freshly prepared 2.3 M sucrose in PBS in a refrigerator for between 8 h and overnight. Pieces of pellet were mounted in fresh sucrose solution on aluminium pins (Leica) plunge frozen into liquid nitrogen and stored. Cryosections (80 nm) were cut on a Leica FCS Ultracut T using a dry diamond knife, collected onto plastic loops containing 2.3 M sucrose in PBS and transferred to formvar carbon-coated glow-discharged 200 hexagonal mesh copper/palladium grids (Agar Scientific) for immunogold labelling, which was performed as follows.

On a strip of Parafilm placed along the laboratory bench, the grids were transferred section-side down onto drops of 0.05 M glycine for 5 min to block free aldehyde groups within the fixed cells and then to 5% or 10% fetal calf serum in PBS (in which blocking medium all subsequent reagents were diluted) for 20 min. The grids are thus moved along from drop to drop in rabbit primary antibody 0.5–500 µg/ml for 1 h, rinsed three times for 5 min each in PBS, incubated in 10 nm protein A gold for 45 min, rinsed five times in PBS for 5 min each, fixed in 2.5% glutaraldehyde in PBS for 10 min, rinsed 10 times in freshly distilled water over 10 min to remove phosphate, contrasted on drops of 2% methyl cellulose and 0.3% uranyl acetate on an ice-chilled metal block in the dark for 10 min, picked up on wire loops and blotted dry. The grids were then viewed on a Philips CM100 transmission electron microscope.

Supplementary data

Supplementary data are available at *The EMBO Journal* Online.

C.L.Allen, D.Goulding and M.C.Field

References

Alexander,D.L., Schwartz,K.J., Balber,A.E. and Bangs,J.D. (2002) Developmentally regulated trafficking of the lysosomal membrane protein p67 in *Trypanosoma brucei*. *J. Cell Sci.*, **115**, 3253–3263.

Bangs,J.D., Andrews,N.W., Hart,G.W. and Englund,P.T. (1986) Posttranslational modification and intracellular transport of a trypanosome variant surface glycoprotein. *J. Cell Biol.*, **103**, 255–263.

Bangs,J.D., Uyetake,L., Brickman,M.J., Balber,A.E. and Boothroyd,J.C. (1993) Molecular cloning and cellular localization of a BiP homologue in *Trypanosoma brucei*. Divergent ER retention signals in a lower eukaryote. *J. Cell Sci.*, **105**, 1101–1113.

Benting,J.H., Rietveld,A.G. and Simons,K. (1999) *N*-glycans mediate the apical sorting of a GPI-anchored, raft-associated protein in Madin-Darby canine kidney cells. *J. Cell Biol.*, **146**, 313–320.

Boehm,M. and Bonifacino,J.S. (2002) Genetic analyses of adaptin function from yeast to mammals. *Gene*, **286**, 175–186.

Brickman,M.J., Cook,J.M. and Balber,A.E. (1995) Low temperature reversibly inhibits transport from tubular endosomes to a perinuclear, acidic compartment in African trypanosomes. *J. Cell Sci.*, **108**, 3611–3621.

Costaguta,G., Stefan,C.J., Bensen,E.S., Emr,S.D. and Payne,G.S. (2001) Yeast Gga coat proteins function with clathrin in Golgi to endosome transport. *Mol. Biol. Cell*, **12**, 1885–1896.

Denny,P.W., Field,M.C. and Smith,D.F. (2001) GPI-anchored proteins and glycoconjugates segregate into lipid rafts in Kinetoplastida. *FEBS Lett.*, **491**, 148–153.

Field,H., Farjah,M., Pal,A., Gull,K. and Field,M.C. (1998) Complexity of trypanosomatid endocytosis pathways revealed by Rab4 and Rab5 isoforms in *Trypanosoma brucei*. *J. Biol. Chem.*, **273**, 32102–32110.

Field,H., Sherwin,T., Smith,A.C., Gull,K. and Field,M.C. (2000) Cell-cycle and developmental regulation of TbRAB31 localisation, a GTP-locked Rab protein from *Trypanosoma brucei*. *Mol. Biochem. Parasitol.*, **106**, 21–35.

Ford,M.G., Mills,I.G., Peter,B.J., Vallis,Y., Praefcke,G.J., Evans,P.R. and McMahon,H.T. (2002) Curvature of clathrin-coated pits driven by epsin. *Nature*, **419**, 361–366.

Geuskens,M., Pays,E. and Cardoso de Almeida,M.L. (2000) The lumen of the flagellar pocket of *Trypanosoma brucei* contains both intact and phospholipase C-cleaved GPI anchored proteins. *Mol. Biochem. Parasitol.*, **108**, 269–275.

Grunfelder,C.G., Engstler,M., Weise,F., Schwarz,H., Stierhof,Y.D., Boshart,M. and Overath,P. (2002) Accumulation of a GPI-anchored protein at the cell surface requires sorting at multiple intracellular levels. *Traffic*, **3**, 547–559.

Grunfelder,C.G., Engstler,M., Weise,F., Schwarz,H., Stierhof,Y.D., Morgan,G.W., Field,M.C. and Overath,P. (2003) Endocytosis of a glycosylphosphatidylinositol-anchored protein via clathrin-coated vesicles, sorting by default in endosomes and exocytosis via Rab11-positive carriers. *Mol. Biol. Cell*, **14**, 2029–2040.

Ilgoutz,S.C. and McConville,M.J. (2001) Function and assembly of the Leishmania surface coat. *Int. J. Parasitol.*, **31**, 899–908.

Jeffries,T.R., Morgan,G.W. and Field,M.C. (2001) A developmentally regulated rab11 homologue in *Trypanosoma brucei* is involved in recycling processes. *J. Cell Sci.*, **114**, 2617–2626.

LaCount,D.J., Bruse,S., Hill,K.L. and Donelson,J.E. (2000) Double-stranded RNA interference in *Trypanosoma brucei* using head-to-head promoters. *Mol. Biochem. Parasitol.*, **111**, 67–76.

LaCount,D.J., Barrett,B. and Donelson,J.E. (2002) *Trypanosoma brucei* FLA1 is required for flagellum attachment and cytokinesis. *J. Biol. Chem.*, **277**, 17580–17588.

Le,P.U., Guay,G., Altschuler,Y. and Nabi,I.R. (2002) Caveolin-1 is a negative regulator of caveolae-mediated endocytosis to the endoplasmic reticulum. *J. Biol. Chem.*, **277**, 3371–3379.

Magalhaes,A.C., Silva,J.A., Lee,K.S., Martins,V.R., Prado,V.F., Ferguson,S.S., Gomez,M.V., Brentani,R.R. and Prado,M.A. (2002) Endocytic intermediates involved with the intracellular trafficking of a fluorescent cellular prion protein. *J. Biol. Chem.*, **277**, 33311–33318.

Maier,A.G., Webb,H., Ding,M., Bremser,M., Carrington,M. and Clayton,C. (2001) The coatomer of *Trypanosoma brucei*. *Mol. Biochem. Parasitol.*, **115**, 55–61.

Merrifield,C.J., Feldman,M.E., Wan,L. and Almers,W. (2002) Imaging actin and dynamin recruitment during invagination of single clathrin-coated pits. *Nat. Cell Biol.*, **4**, 691–698.

Morgan,G.W., Allen,C.L., Jeffries,T.R., Hollinshead,M. and Field,M.C. (2001) Developmental and morphological regulation of clathrin-mediated endocytosis in *Trypanosoma brucei*. *J. Cell Sci.*, **114**, 2605–2615.

Morgan,G.W., Hall,B.S., Denny,P.W., Carrington,M. and Field,M.C. (2002a) The endocytic apparatus of the kinetoplastida. Part I: a dynamic system for nutrition and evasion of host defences. *Trends Parasitol.*, **18**, 491–496.

Morgan,G.W., Hall,B.S., Denny,P.W., Field,M.C. and Carrington,M.C. (2002b) The endocytic apparatus of the kinetoplastida. Part II: machinery and components of the system. *Trends Parasitol.*, **18**, 540–546.

Nichols,B.J. and Lippincott-Schwartz,J. (2001) Endocytosis without clathrin coats. *Trends Cell Biol.*, **11**, 406–412.

Nolan,D.P. *et al.* (2000) Characterization of a novel alanine-rich protein located in surface microdomains in *Trypanosoma brucei*. *J. Biol. Chem.*, **275**, 4072–4080.

O'Beirne,C., Lowry,C.M. and Voorheis,H.P. (1998) Both IgM and IgG anti-VSG antibodies initiate a cycle of aggregation–disaggregation of bloodstream forms of *Trypanosoma brucei* without damage to the parasite. *Mol. Biochem. Parasitol.*, **91**, 165–193.

Pal,A., Hall,B.S., Nesbeth,D.N., Field,H.I. and Field,M.C. (2002) Differential endocytic functions of *Trypanosoma brucei* Rab5 isoforms reveal a glycosylphosphatidylinositol-specific endosomal pathway. *J. Biol. Chem.*, **277**, 9529–9539.

Pal,A., Hall,B.S., Jeffries,T.R. and Field,M.C. (2003) Rab5 and Rab11 mediate transferrin and anti-variant surface glycoprotein antibody recycling in *Trypanosoma brucei*. *Biochem. J.*, **374**, 443–451.

Payne,G.S., Hasson,T.B., Hasson,M.S. and Schekman,R. (1987) Genetic and biochemical characterization of clathrin-deficient *Saccharomyces cerevisiae*. *Mol. Cell. Biol.*, **7**, 3888–3898.

Sabharanjak,S., Sharma,P., Parton,R.G. and Mayor,S. (2002) GPI-anchored proteins are delivered to recycling endosomes via a distinct cdc42-regulated, clathrin-independent pinocytic pathway. *Dev. Cell*, **2**, 411–423.

Seeger,M. and Payne,G.S. (1992) A role for clathrin in the sorting of vacuolar proteins in the Golgi complex of yeast. *EMBO J.*, **11**, 2811–2818.

Takei,K. and Haucke,V. (2001) Clathrin-mediated endocytosis: membrane factors pull the trigger. *Trends Cell Biol.*, **11**, 385–391.

van den Hoff,M.J., Moorman,A.F. and Lamers,W.H. (1992) Electroporation in 'intracellular' buffer increases cell survival. *Nucleic Acids Res.*, **20**, 2902.

Wang,J., Gunning,W., Kelley,K.M. and Ratnam,M. (2002) Evidence for segregation of heterologous GPI-anchored proteins into separate lipid rafts within the plasma membrane. *J. Membr. Biol.*, **189**, 35–43.

Wang,Z., Morris,J.C., Drew,M.E. and Englund,P.T. (2000) Inhibition of *Trypanosoma brucei* gene expression by RNA interference using an integratable vector with opposing T7 promoters. *J. Biol. Chem.*, **275**, 40174–40179.

Wettey,F.R., Hawkins,S.F., Stewart,A., Luzio,J.P., Howard,J.C. and Jackson,A.P. (2002) Controlled elimination of clathrin heavy-chain expression in DT40 lymphocytes. *Science*, **297**, 1521–1525.

Wirtz,E., Leal,S., Ochatt,C. and Cross,G.A. (1999) A tightly regulated inducible expression system for conditional gene knock-outs and dominant-negative genetics in *Trypanosoma brucei*. *Mol. Biochem. Parasitol.*, **99**, 89–101.

Yeung,B.G., Phan,H.L. and Payne,G.S. (1999) Adaptor complex-independent clathrin function in yeast. *Mol. Biol. Cell*, **10**, 3643–3659.